Sensors and Actuators B 251 (2017) 842–850

Contents lists available at ScienceDirect

Sensors and Actuators B: Chemical

journal homepage: www.elsevier.com/locate/snb

Nickel plasma modification of graphene for high-performance non-enzymatic glucose sensing

Hao Wu[a], Yu Yu[b], Wenyu Gao[b], Ang Gao[a], Abdul Mateen Qasim[a], Fan Zhang[a], Junzhong Wang[c], Kejian Ding[b,*], Guosong Wu[a], Paul K. Chu[a,*]

[a] Department of Physics and Materials Science, City University of Hong Kong, Tat Chee Avenue, Kowloon, Hong Kong, China
[b] School of Science, Beijing Jiaotong University, Beijing 100044, PR China
[c] Key Laboratory of Carbon Materials, Institute of Coal Chemistry, Chinese Academy of Science, Taiyuan 030001, PR China

ARTICLE INFO

Article history:
Received 13 March 2017
Received in revised form 15 May 2017
Accepted 23 May 2017
Available online 25 May 2017

Keywords:
Glucose sensor
Nickel
Plasma modification
Grapheme

ABSTRACT

A Ni plasma-modified graphene-based glucose sensor is prepared on a glassy carbon electrode. The Ni plasma-modified graphene, which has structural integrity and good conductivity after the plasma treatment, shows excellent glucose sensing ability as confirmed by electrochemical assessment of the GC-G-Ni electrode. The GC-G-Ni sensor exhibits a high glucose sensitivity of 2213 $\mu A\,mM^{-1}\,cm^{-2}$, low detection limit of 1 μM, short response time of less than 1 s, good selectivity, long-term stability, and reproducibility. The fabrication method and strategy are promising to large-scale production of electrochemical biosensors based on transition elements.

1. Introduction

Glucose sensing has received much attention due to its significance in the food industry, biotechnology, and clinical diagnosis [1]. Although traditional electrochemical glucose sensors based on the glucose oxidase enzyme have good selectivity, sensitivity, and fast response, clinical application of enzymatic sensors is hindered by the intrinsic limitations of the enzyme [2,3]. In this respect, non-enzymatic sensors have attracted research interests and transition metals and their oxides (Au, Pt, Co, Cu, Ni, Co_3O_4, Cu_2O, NiO, RuO_2) have been used in electrochemical oxidation of glucose [4–11]. Among them, Ni and its oxide have been extensively investigated on account of the low cost and good performance. Many Ni-based non-enzymatic glucose sensors have been constructed by modifying the substrates with nickel-based nanomaterials or nanocomposites, for example, nano nickel oxide [12], nickel oxide nanoflake arrays [13], nickel-carbon nanotube hybrids [14,15], nickel-graphene hybrids [16,17], nickel hydroxide-nanodiamond [18], and nickel nanowires [19,20]. Compared to bulk electrodes, electrodes modified with these nanomaterials deliver better performance due to the large surface area and rapid mass transport. However, practical application of these nanomaterials-based sensors is still hampered by the complicated fabrication process and inconvenience in large-scale batch manufacturing.

Graphene produced by exfoliation from pyrolytic graphite is an allotrope of carbon with a unique 2D nanostructure in which the carbon atoms are covalently bonded in a sp^2 network [21]. Owing to the large specific surface area and excellent conductivity, graphene has large potential in applications such as sensors, energy storage materials, and electronic devices [21–24]. However, graphene is mostly used in the form of reduced graphene oxide which conductivity is not as good as that of pristine graphene. Moreover, further application of graphene is hindered by the high price and inefficient production [25]. In this work, pristine graphene synthesized by a high-yield electrochemical expansion method [26] is used as a substrate instead of reduced graphene oxide to improve the performance and lower the preparation cost and complexity.

Plasma surface modification is a common approach to improve the surface properties and performance of functional materials and devices [27–32]. In this technique, metallic and gaseous elements are implanted into or deposited into a variety of substrates controllably. It is also a batch processing technique suitable for large-scale production for the functional coatings and microelectronics industry [33]. Gaseous plasma treatment has been conducted on graphene and graphene oxide to enhance the photoelectric and catalytic properties [34–39]. Nevertheless, the effects of metal plasma processing on nanomaterials such as graphene

* Corresponding authors.
E-mail addresses: dkjian@bjtu.edu.cn (K. Ding), paul.chu@cityu.edu.hk (P.K. Chu).

http://dx.doi.org/10.1016/j.snb.2017.05.128
0925-4005/

have not been extensively studied. Moreover, since the plasma treatment involves energetic ion bombardment, the conditions must be optimized to yield the pre-designed properties while not producing undesirable damage to the nanomaterials. In this work described in this paper, nickel ion-plasma treatment is performed on pristine graphene and the glucose sensing capability is evaluated.

2. Experimental details

2.1. Chemicals and reagents

The graphene flakes were produced by electrochemical expansion of graphite with lithium perchlorate in the propylene carbonate electrolyte as described in the literature [26]. The chemical reagents including sodium hydroxide (NaOH), D-(+)-Glucose, L-ascorbic acid (AA), uric acid (UA), dopamine, and L-lactic acid (LA) were purchased from International Laboratory (IL, USA) and used as received.

2.2. Ni plasma modification and preparation of the GC-G-Ni electrode

The glassy carbon (GC) electrode (3 mm in diameter) was polished with 0.05 μm alumina slurry, rinsed thoroughly with deionized water, and dried with nitrogen gas. 5 mg of graphene were dispersed in 2 mL of ethanol and ultra-sonicated for 30 min to obtain a homogeneous solution. 2 μL of the graphene dispersion were drop-cast on a glassy carbon electrode and dried with nitrogen. The graphene-GC electrode was used as a substrate in the subsequent nickel plasma treatment.

Ni plasma modification was conducted on the plasma immersion ion implantation and deposition (PIII&D) system in the Plasma Laboratory of City University of Hong Kong (Fig. S1). A nickel rod (99.99%) was used as the cathodic arc plasma source. Both the GC and GC-G electrodes were put in the vacuum chamber which was evacuated to a pressure of 5×10^{-3} Pa. Argon was bled into the chamber at a flow rate of 30 sccm to a working pressure of 2×10^{-1} Pa. The Ni plasma was generated by the pulse filtered cathode arc source and a bias voltage of 400 V was applied to the sample. The plasma treatment time was for 0.5 h and the Ni fluence was calculated by the following relationship:

$$D\left(\text{ions}/cm^2\right) = k\frac{I_m \cdot \tau \cdot n}{e \cdot S \cdot \overline{n_0}}, \quad (1)$$

where k is the calibration factor, I_m is the average current (A), τ is the pulse duration (s), n is the pulse number, e is the electron charge (1.602×10^{-19} Coulomb), S is the sample area (cm^2), and $\overline{n_0}$ is average valence.

2.3. Characterization

The GC-G and GC-G-Ni electrodes were characterized by field-emission scanning electrode microscopy and energy-dispersive X-ray spectrometry (FE-SEM; JEOL JSM-7001F). Atomic force microscopy (AFM; Auto Probe CP, Park Scientific Instruments, USA) was used to determine the surface morphology before and after the plasma treatment. The Raman scattering spectra were acquired using a 514.5 nm argon laser (Horiba LabRAM) and X-ray photoelectron spectroscopy (XPS; Physical Electronics PHI 5802) with Al K_α irradiation was carried out to determine the chemical states.

2.4. Electrochemical evaluation

Cyclic voltammetry (CV) and amperometric measurements were carried out in 0.1 mM NaOH on a CHI 570B electrochemical workstation (Shanghai, China). The three-electrode cell (80 mL) comprised a modified glassy carbon electrode (GC) as the working electrode, Ag/AgCl (saturated KCl) electrode as the reference electrode, and platinum wire as the counter electrode. Electrochemical impedance spectroscopy (EIS) was conducted in an electrolyte containing 0.1 mM KCl and 50 mM $[Fe(CN)_6^{4-/3-}]$ in the frequency range between 0.1 and 100,000 Hz with an amplitude of 5 mV. All the measurements were carried out at room temperature.

3. Results and discussion

3.1. Characterization

AFM and SEM are employed to observe the morphology of graphene before and after the Ni plasma treatment. As shown in the AFM images of graphene (Fig. 1a) and Ni plasma-treated graphene (Fig. 1b), the surface becomes rougher after the plasma process with the average roughness increasing from 0.465 nm to 1.78 nm. The low-resolution SEM images in Fig. 1c and d reveal no obvious structural change on the plasma-treated graphene. However, as shown by the inset high-resolution images, the Ni-plasma treated graphene has a rougher surface than graphene with nano-scale protrusions and ridge-like structures. EDS shows that the average Ni concentration of the plasma-treated graphene is 3.9% (no Ni detected from the untreated graphene in Fig. S2a) and the EDS elemental maps (Figs. S2b–g) show that Ni is evenly distributed on the plasma-treated graphene. Raman scattering is performed to determine the quality of graphene by monitoring the relative intensity of the D peak (defects related) and G peak (E_{2g} photon of C sp^2 atoms). As shown in Fig. 1(f), the pristine graphene shows an I_D/I_G ratio of <0.2 indicating a small defect concentration. After the low-energy Ni plasma treatment (400 V), the structure is preserved showing little plasma-induced damage. In comparison, graphene subjected to high-energy ion implantation shows a Raman spectrum with higher I_D/I_G ratio and damaged surface morphology (Fig. S3a and b). Hence, the low-energy plasma treatment does not create significant damage in graphene.

Fig. 2(a) shows the Nyquist plots of the bare GCE, GC-G electrode, GC-G-Ni electrode, and GC-Ni electrode. The high frequencies are related to the electron transfer limited process and the low frequencies are associated with the diffusion process. An equivalent circuit $R_s(CPE_1(R_{ct}CPE_2))$ is implemented to fit the EIS data and determine the charge transfer resistance (R_{ct}) as shown in Table S1. After graphene introduction, the GC-G electrode shows a smaller R_{ct} (141.8 ± 6.8 ohm) than the bare GCE (554.3 ± 9.4 ohm) indicating an improved electron transfer rate of $[Fe(CN)_6]^{3-/4-}$ [40]. After the Ni plasma treatment, R_{ct} of the GC-G-Ni electrode decreases to 95.6 ± 2.0 ohm and that of the R_{ct} GC-Ni electrode drops to 339.5 ± 7.7 ohm. Similar results have also been reported after modification with Ni nanoparticles [41] and NiO NPs [42] and the decrease in R_{ct} caused by Ni can be attributed to the good electron transfer ability of the plasma-treated Ni.

CV is performed to activate the electrode until it reaches the optimal performance and remains stable. As shown in Fig. 2(b), the GC-G-Ni electrode is subjected to a voltage range of −1.0 to 1.5 V in 0.1 M NaOH at a scanning rate of 100 mV/s. After 200 cycles, the cyclic voltammograms stabilize. The increasing baseline current during CV arises from oxidation of metallic Ni to $Ni(OH)_2$ in the alkali medium. The anodic peaks at 0.51–0.54 V and cathodic peaks at 0.38–0.42 V can be assigned to the redox couple of Ni(II)/Ni(III) [43]. The increased peak currents during scanning indicate progres-

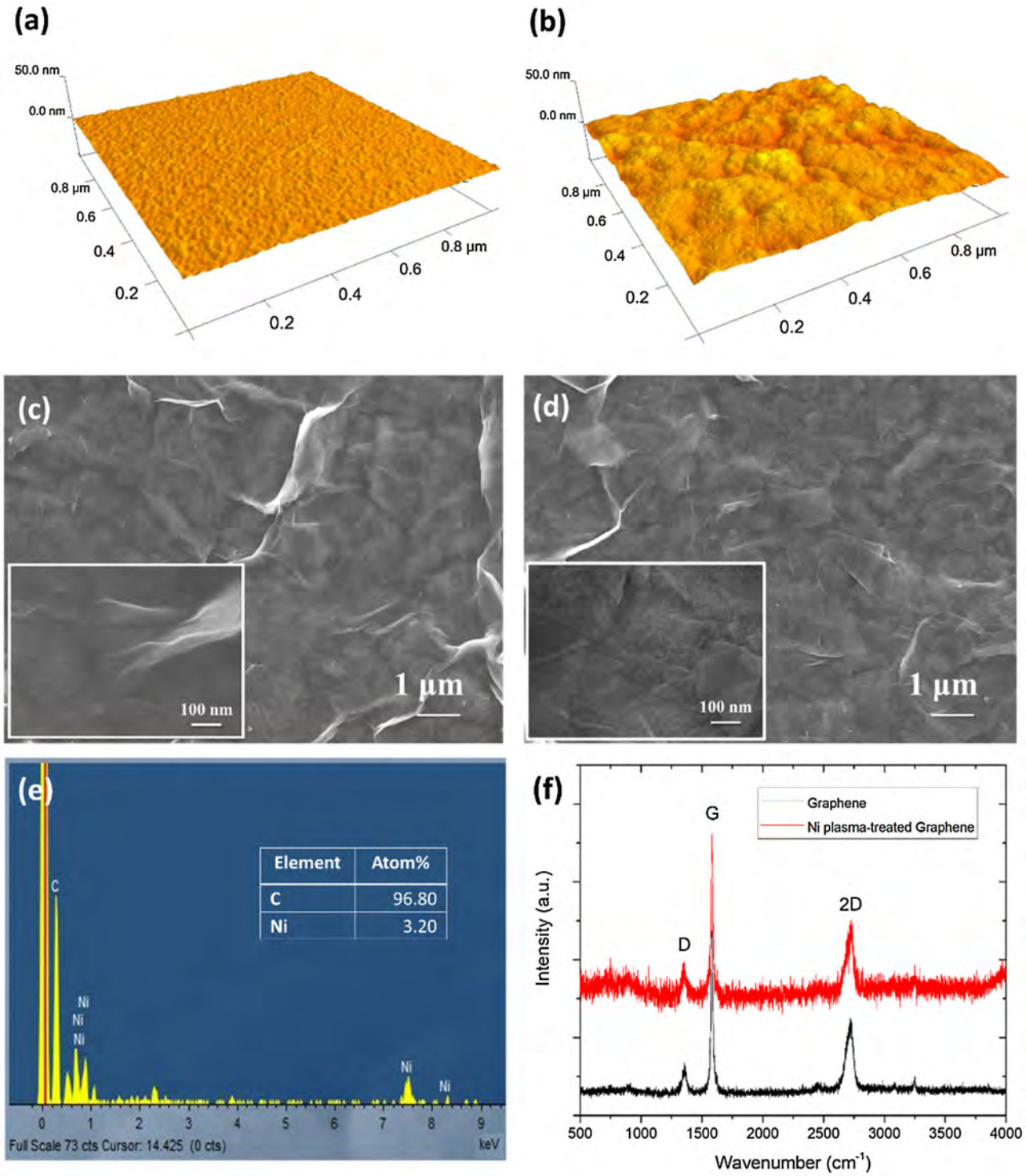

Fig. 1. AFM images of (a) graphene and (b) Ni plasma-treated graphene; SEM pictures of (c) graphene and (d) Ni plasma-treated graphene with the inset showing the magnified surface by SEM; (e) EDS scan of the Ni plasma-treated graphene; (f) Raman scattering spectra of graphene and Ni plasma-treated graphene.

sive enrichment of the accessible electroactive species Ni(II)/Ni(III) on the graphene surface [44]. The surface chemical composition and states are determined by X-ray photoelectron spectroscopy (XPS). As shown in Fig. 2(c), the XPS survey scans of GC-G-Ni before and after activation show peaks corresponding to C, O, and Ni. The relative intensity of the O1s peak and O Auger peak increases implying that oxidation takes place in the activation process. The high-resolution XPS spectra of Ni2p are shown in Fig. 2(d). After activation, the intensity of the Ni $2p_{3/2}$ and $2p_{1/2}$ peaks decreases and new $Ni(OH)_2$ and NiOOH peaks appear indicating that Ni is oxidized. The Ni $2p_{3/2}$ peaks before and after activation are deconvoluted as shown in Fig. 2(e) and (f). Ni^0 and the satellite peak can be observed from GC-G-Ni and a small quantity of NiO is detected because of oxidation in air. Despite the existence of NiO, the deposited Ni is basically metallic. However, after CV activation,

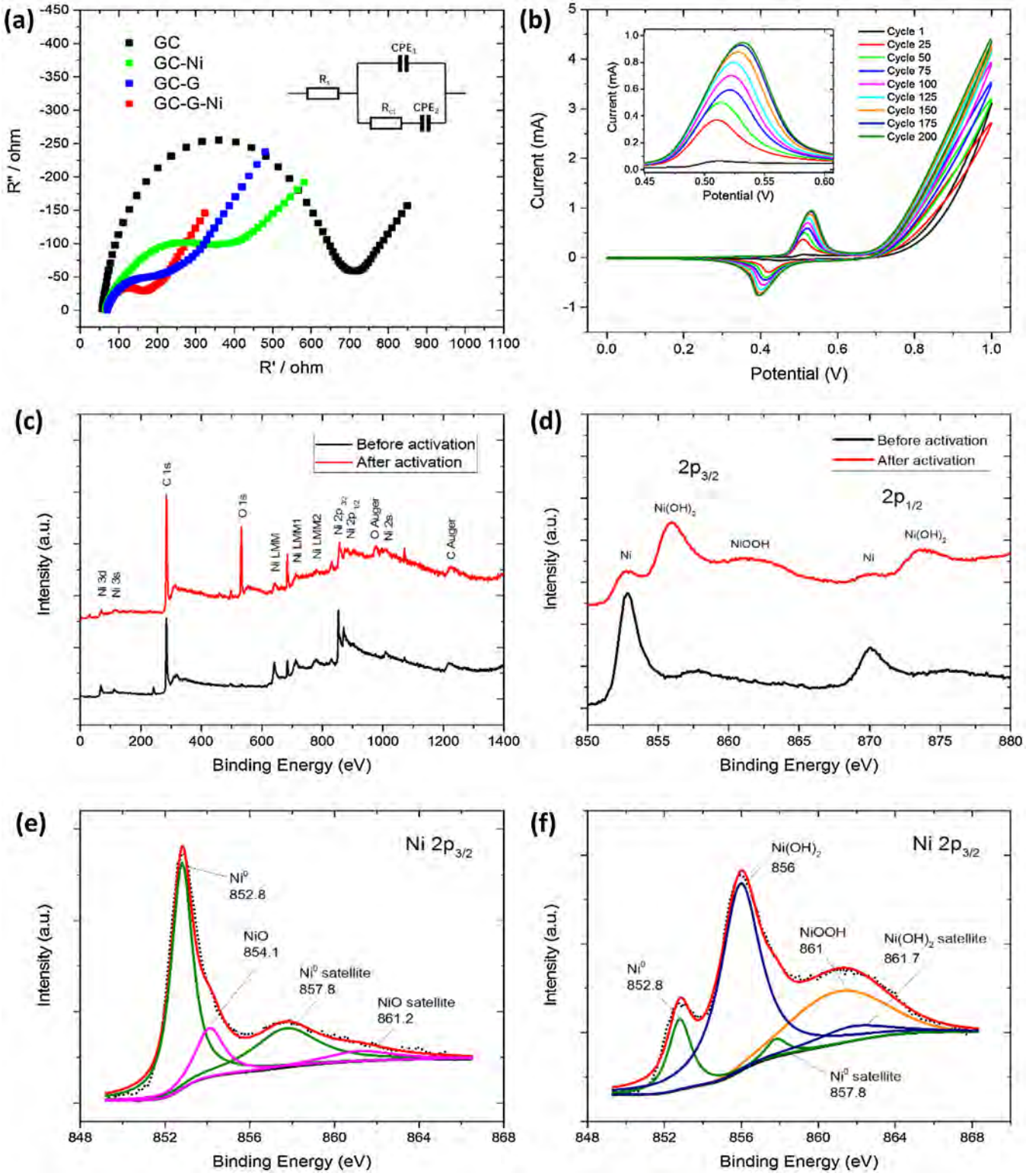

Fig. 2. (a) EIS Nyquist plots acquired in the solution containing 10 mM $[Fe(CN)_6]^{3-/4-}$ in 0.1 M KCl electrolyte; (b) CV plot during activation of GC-G-Ni electrode; (c) XPS survey scans and (d) High-resolution XPS spectra of the GC-G-Ni electrode before and after activation; High-resolution Ni $2p_{3/2}$ XPS spectra of the GC-G-Ni electrode (e) before and (f) after activation.

most of the metallic Ni is oxidized to $Ni(OH)_2$ and NiOOH. The CV activation process can be expressed as follows [45]:

$$Ni + 2OH^- - 2e^- \rightarrow Ni(OH)_2, \quad (2)$$

$$Ni(OH)_2 + OH^- \rightarrow NiOOH + H_2O + e^-. \quad (3)$$

3.2. Electrochemical characteristics of the GC-G-Ni electrode

To study the CV propeties of GC-G-Ni electrode, a Ni-plasma treated GC electrode (GC-Ni) is used for comparison. As shown in Fig. 3(a), after addition of 1 mM glucose, the anodic peak current

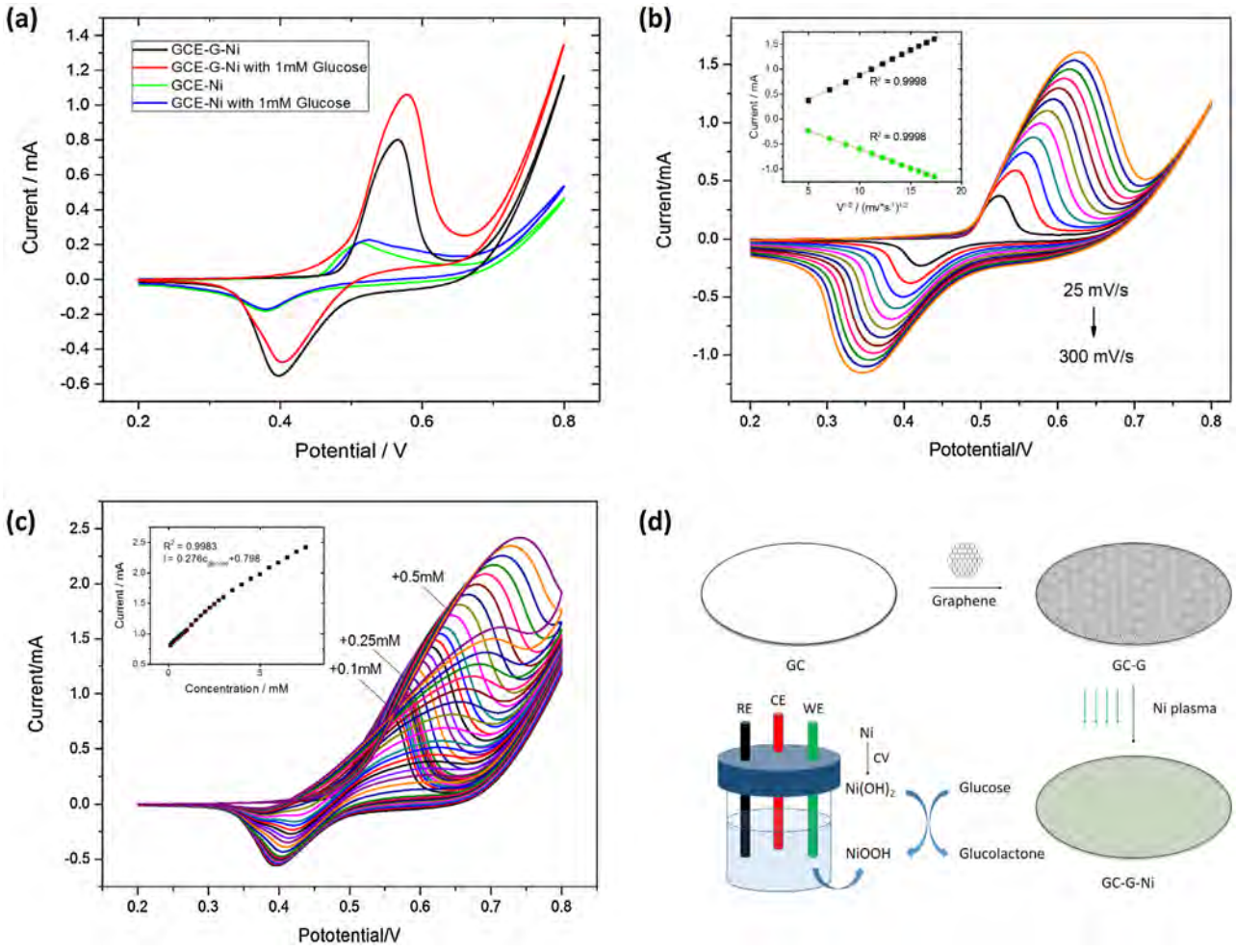

Fig. 3. (a) Cyclic voltammograms of the GC-Ni and GC-G-Ni electrodes at a scanning rate of 100 mV/s in 0.1 M NaOH; (b) Cyclic voltammograms of the GC-G-Ni electrode at different scanning rates in 0.1 M NaOH with the inset showing the anodic and cathodic peak currents as a function of square root of the scanning rates; (c) Cyclic voltammograms of the GC-G-Ni electrode in 0.1 M NaOH with glucose concentrations increased from 0.1 mM to 1.0 mM with a stepwise increment of 0.1 mM, from 1.0 mM to 3 mM with a stepwise increment of 0.25 mM, and from 3.0 mM to 7.0 mM with a stepwise increment of 0.5 mM. The inset shows the anodic peak currents as a function of glucose concentration; (d) Schematic illustration of the fabrication process and detection by the GC-G-Ni glucose sensor.

of the GC-G-Ni electrode increases simultaneously with a slightly positive shift of the peak potential. The GC-Ni electrode is also CV-activated prior to evaluating the CV response to 1 mM glucose. After addition of 1 mM glucose, the anodic current increases and a smaller starting potential for glucose oxidation is observed from GC-G-Ni in comparison with GC-Ni. The current response of the GC-G-Ni electrode is 16.6 times larger (from 0.016 mA to 0.266 mA) than that of the GC-Ni electrode, suggesting glucose electrocatalysis is enhanced by graphene. This stems from the excellent conductivity and large surface area of graphene subsequently providing more interactive sites for the Ni(II)/Ni(III) redox couple. The CV current response in 1 mM glucose of the GC-G-Ni-HI electrode is also monitored (0.064 mA) and it is 76% smaller than that of the GC-G-Ni electrode.

The CV properties of the GC-G-Ni electrode at different scanning rates in 1 M NaOH are investigated. As shown in Fig. 3(b), both the redox and oxidation currents increase as the scanning rates are increased from 25 mV/s to 300 mV/s. The peaks can be assigned to the redox reaction of Ni^{3+}/Ni^{2+} couple on the electrode surface [46] as follows:

$$\text{Anodicpeak}: Ni(OH)_2 + OH^- \rightarrow NiOOH + H_2O + e^- \quad (4)$$

$$\text{Cathodicpeak}: NiOOH + H_2O + e^- \rightarrow Ni(OH)_2 + OH^-. \quad (5)$$

A linear dependence between the peak currents and the square root of the scanning rates can be established for both the anodic and cathodic peak currents signifying the diffusion-controlled electrochemical kinetics [47]. It obeys the Randles–Sevcik condition for the diffusion-controlled electrode reaction [48–50]:

$$i_P = \left(2.686 \times 10^5\right) n^{3/2} A D^{1/2} C \nu^{1/2}, \quad (6)$$

where, i_P represents the peak current, n represents the number of electrons involved, A represents the electrode area (cm^2), D represents the diffusion coefficient ($cm^2{*}s^{-1}$), C represents the concentration (mol/cm^3), and ν stands for the scanning rate (V/s). The anodic peak potential shifts positively while the cathodic potential shifts negatively with increasing scanning rates generating a larger peak-to-peak potential separation.

Electrochemical oxidation of glucose is investigated in 0.1 M NaOH at a scanning rate of 100 mV/s. As shown in Fig. 3(c), the anodic current in the positive scan increases gradually with glucose concentration. Oxidation of glucose is electrocatalyzed by the $NiOOH/Ni(OH)_2$ redox couple according to the following reaction [13,51,52]:

$$NiOOH + \text{glucose} \rightarrow Ni(OH)_2 + \text{glucolactone}, \quad (7)$$

In the CV measurement of glucose with increasing concentration, the increase of anodic current can be attributed to

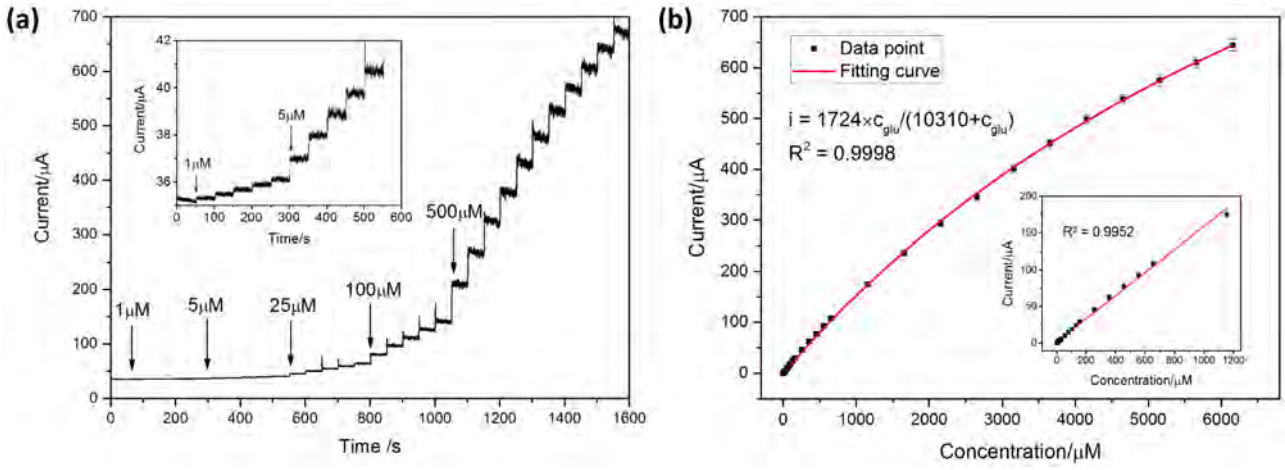

Fig. 4. (a) Amperometric current response of the GCE-G-Ni during addition of 1 μM, 5 μM, 25 μM, 100 μM, and 500 μM glucose at an applied potential of 0.6 V; (b) Calibration curve of the response current versus glucose concentration.

Table 1
Comparison of the results pertaining to glucose detection for non-enzymatic Ni-based electrodes.

Electrode	Sensitivity ($\mu A\,mM^{-1}\,cm^{-2}$)	Linear range (μM)	LOD (μM)	Response time	Reference
Ni-CNT	1384.1	5–2000	2	3	[13]
NA/NiONF-rGO/GCE	1100	2–600	0.77	5	[54]
NiONPs/GO/GC	1087	3.13–3050	1	Not mentioned	[35]
Chitosan-rGO-NiNPs	318.4	up to 9000	4.1	Not mentioned	[40]
Ni-rGO	813	1–110	1	<5	[15]
NiNPs/ATP/RGO	1414.4	1–710	0.37	2	[55]
Ni-SWCNTs	907	1–900	0.3	2	[58]
Ni powder/CCE	0.04	0.5–5000	0.1	<1	[59]
$Ni(OH)_2/TiO_2$	192	30–14000	8	<1	[60]
Nano NiO	55.9	1–110	0.16	<5	[10]
Ni-ITO	189.5	1–350	0.5	Not mentioned	[44]
GCE-Graphene-Ni	2213	1–1150	0.1	1	This work

electro-oxidation of glucose catalysed by Ni-graphene composite and subsequent oxidation of $Ni(OH)_2$ to NiOOH. Electro-oxidation of glucose also consumes NiOOH and decreases the cathodic peak current [53]. Meanwhile, the anodic peak shifts positively as the glucose concentration increases. This phenomenon can be explained by the nucleation of NiOOH and increased active sites for the Ni(III) and Ni(II) species [54]. The peak shift has been ascribed to adsorption of glucose and oxidized intermediates on active sites of the Ni-based materials causing kinetics limitation in the corresponding reactions [55,56]. As shown in the inset plot in Fig. 3(c), the redox current shows a good linear relationship with glucose concentration in the range between 0.55 V and 0.65 V. The anodic current varies linearly with the glucose concentration between 100 μM and 3 mM with a correlation coefficient of 0.9983.

3.3 Amperometric determination of glucose by the GC-G-Ni electrode

Amperometric determination of glucose is performed by chronoamperometry. The amperometric response of the GC-G-Ni electrode to glucose is monitored at a potential of 0.6 V under constant stirring. As shown in Fig. 4(a), the GC-G-Ni electrode shows a sensitive and rapid response. A low detection limit of 1 μM at a signal-to-noise (S/N) ratio of 3 is observed. The corresponding calibration plot shows a linear relationship between 1 and 1150 μM with a slope of 0.1571 $\mu A\,\mu M^{-1}$ and correlation coefficient of 0.9952. The sensitivity of the GC-G-Ni sensor is calculated to be 2213 $\mu A\,mM^{-1}\,cm^{-2}$ by dividing the slope of the linear fitted equation by the electrode surface area (0.071 cm^2). As electrochemical oxidation of glucose on the electrode is a surface catalytic reaction [15,57–59], the Langmuir isothermal theory can be utilized to fit the calibration curve [57,60] and the concentration of glucose on the sensor electrode (c_{glu-A}) can be expressed as:

$$C_{glu-A} = \frac{K_A c_{glu} c_t}{1 + K_A c_{glu}}, \tag{8}$$

where c_{glu} is the glucose concentration in the electrolyte, c_t is the total molar concentration in the active sites on the GC-G-Ni electrode being constant, and K_A is the adsorption equilibrium constant. The current response in electrochemical oxidation of glucose should be proportional to the glucose concentration adsorbed on the electrode (c_{glu-A}) with a rate constant of K_1 and i can be expressed as:

$$i = K_1 c_{glu-A} = \frac{K_1 K_A c_t c_{glu}}{1 + K_A c_{glu}} = \frac{K_B c_{glu}}{1 + K_A c_{glu}}, \tag{9}$$

According to the fitted results (Fig. 4b), $K_B = 0.1672$, $K_A = 9.67^{*}10^{-5}$, and $i = 0.1672 c_{glu}/(1 + 9.67^{*}10^{-5} c_{glu})$ with a correlation coefficient of 0.9998. When the glucose concentration is low enough (i.e. $c_{glu} < 1mM$), the equation can be approximated as $i = 0.1524 c_{glu}$ and the sensitivity is 2147 $\mu A\,mM^{-1}\,cm^{-2}$, being in good agreement with the sensitivity calculated by linear fitting in the linear range. The sensitivity is higher than that observed previously from Ni-based non-enzymatic glucose sensors and the other characteristics are also favorable (Table 1). The high sensitivity and short response time arise from the excellent conductivity of graphene which provides a low-resistance pathway, promotes electron transfer, and reduces the response time [14]. Graphene is a good catalyst support for oxidation of glucose for Ni-based glucose sensors [17,61–63] and the excellent performance described here stems from the large surface-area/volume ratio of uniform

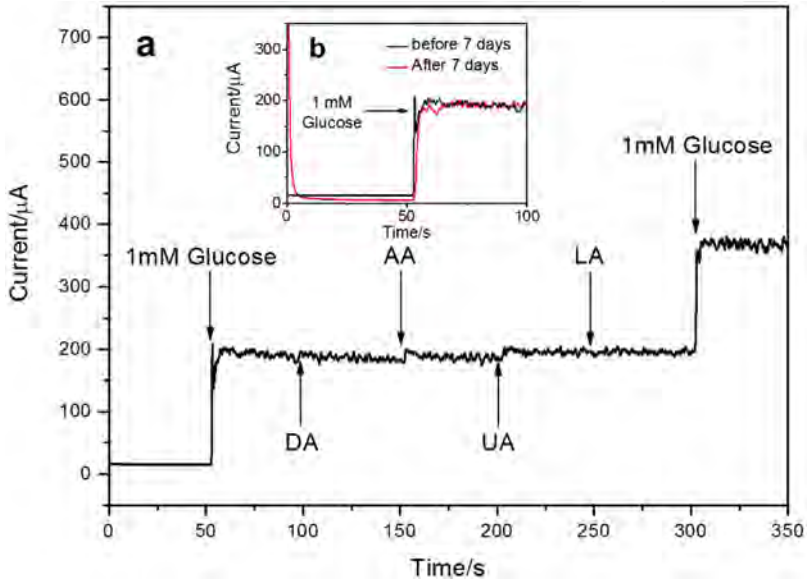

Fig. 5. Interference assessment performed on the GCE-G-Ni electrode in 0.1 M NaOH at 0.6 V with addition of 1 mM glucose, 0.1 mM dopamine (DA), 0.1 mM ascorbic acid (AA), 0.1 mM uric acid (UA), 0.1 mM lactic acid (LA), and 1 mM glucose. The inset shows the amperiometric current response of the GCE-G-Ni electrode in 1 mM glucose after 7 days.

Ni-graphene as well as synergistic effects rendered by Ni and graphene [15,42,63].

3.4. Selectivity, reproducibility, and long-term stability of the GC-G-Ni glucose sensor

Selectivity is of great significance to glucose biosensors especially non-enzymatic sensors because other small molecules such as ascorbic acid (AA) and uric acid (UA) can also be oxidized together with glucose causing interference to elevate the detection limits. The blood glucose level in a normal human is between 4 mM and 7 mM [64], but those of endogenous small molecules are smaller, for example, 0.125 mM for AA, 0.33 mM for UA, [65] and less than 0.13 nM for dopamine. As shown in Fig. 5(a), 0.1 mM dopamine (DA), 0.1 mM ascorbic acid (AA), 0.1 mM uric acid (UA), and 0.1 mM lactic acid (LA) are successively added to monitor the effects of interference to 1 mM glucose. Large current responses are obtained after addition of glucose while the introduction of interfering species such as UA and AA only produce small responses (~5% relative to 1 mM glucose) and the added LA and DA also don't cause significant responses. It should be noted that the relative amounts of UA and AA in real blood are lower than those in our experiment and so the practical impact is negligible. The results indicate that the GC-G-Ni electrode possesses sufficient selectivity in glucose sensing in practice. The long-term stability is also important to glucose sensing and the electrode after sitting in air for 7 days is re-evaluated. As shown in Fig. 5(b), the current response is maintained signifying good long-term stability. The reproducibility is also investigated. Six consecutive amperometric measurements in 5 μM glucose by a single GC-G-Ni electrode show a relative standard deviation (RSD) of 3.82%. A batch test with 4 independently prepared electrodes gives a relative standard deviation of 6.44% to 100 μM glucose from the amperometric measurements (Fig. S4). Hence, the GC-G-Ni glucose sensor possesses good selectivity, stability, and reproducibility.

4. Conclusion

Nickel plasma treatment is conducted to non-destructively modify graphene to produce a nickel-graphene based glucose sensor. The GC-G-Ni sensor has good sensitivity, broad sensing range, and good stability in glucose sensing. As a simple, cost-effective, and scalable method, plasma modification is valuable to large-scale manufacturing of electrochemical biosensors and devices.

Acknowledgements

The work was financially supported by Hong Kong Research Grants Council (RGC) General Research Funds (GRF) No. CityU 11301215, City University of Hong Kong Strategic Research Grant (SRG) No. 7004188, and the National Natural Science Foundation of China (Grants 11079010, 21373255).

Appendix A. Supplementary data

Supplementary data associated with this article can be found, in the online version, at http://dx.doi.org/10.1016/j.snb.2017.05.128.

References

[1] A. Chen, S. Chatterjee, Nanomaterials based electrochemical sensors for biomedical applications, Chem. Soc. Rev. 42 (2013) 5425–5438.
[2] R. Ahmad, M. Vaseem, N. Tripathy, Y.-B. Hahn, Wide linear-range detecting nonenzymatic glucose biosensor based on CuO nanoparticles inkjet-printed on electrodes, Anal. Chem. 85 (2013) 10448–10454.
[3] Y. Zhang, Y. Li, W. Wu, Y. Jiang, B. Hu, Chitosan coated on the layers' glucose oxidase immobilized on cysteamine/Au electrode for use as glucose biosensor, Biosens. Bioelectron. 60 (2014) 271–276.
[4] Y. Xian, Y. Hu, F. Liu, Y. Xian, H. Wang, L. Jin, Glucose biosensor based on Au nanoparticles–conductive polyaniline nanocomposite, Biosens. Bioelectron. 21 (2006) 1996–2000.
[5] D. Zhai, B. Liu, Y. Shi, L. Pan, Y. Wang, W. Li, et al., Highly sensitive glucose sensor based on Pt nanoparticle/polyaniline hydrogel heterostructures, ACS Nano 7 (2013) 3540–3546.
[6] X.-C. Dong, H. Xu, X.-W. Wang, Y.-X. Huang, M.B. Chan-Park, H. Zhang, et al., 3D graphene–cobalt oxide electrode for high-performance supercapacitor and enzymeless glucose detection, ACS Nano 6 (2012) 3206–3213.
[7] Y. Ding, Y. Wang, L. Su, M. Bellagamba, H. Zhang, Y. Lei, Electrospun Co 3 O 4 nanofibers for sensitive and selective glucose detection, Biosens. Bioelectron. 26 (2010) 542–548.
[8] R.M. Tehrani, S. Ab Ghani, MWCNT-ruthenium oxide composite paste electrode as non-enzymatic glucose sensor, Biosens. Bioelectron. 38 (2012) 278–283.
[9] H.-X. Wu, W.-M. Cao, Y. Li, G. Liu, Y. Wen, H.-F. Yang, et al., In situ growth of copper nanoparticles on multiwalled carbon nanotubes and their application

as non-enzymatic glucose sensor materials, Electrochim. Acta 55 (2010) 3734–3740.
[10] M. Liu, R. Liu, W. Chen, Graphene wrapped Cu2O nanocubes: non-enzymatic electrochemical sensors for the detection of glucose and hydrogen peroxide with enhanced stability, Biosens. Bioelectron. 45 (2013) 206–212.
[11] X. Gao, Y. Lu, M. Liu, S. He, W. Chen, Sub-nanometer sized Cu 6 (GSH) 3 clusters: one-step synthesis and electrochemical detection of glucose, J. Mater. Chem. C 3 (2015) 4050–4056.
[12] Y. Mu, D. Jia, Y. He, Y. Miao, H.-L. Wu, Nano nickel oxide modified non-enzymatic glucose sensors with enhanced sensitivity through an electrochemical process strategy at high potential, Biosens. Bioelectron. 26 (2011) 2948–2952.
[13] G. Wang, X. Lu, T. Zhai, Y. Ling, H. Wang, Y. Tong, et al., Free-standing nickel oxide nanoflake arrays: synthesis and application for highly sensitive non-enzymatic glucose sensors, Nanoscale 4 (2012) 3123–3127.
[14] H. Nie, Z. Yao, X. Zhou, Z. Yang, S. Huang, Nonenzymatic electrochemical detection of glucose using well-distributed nickel nanoparticles on straight multi-walled carbon nanotubes, Biosens. Bioelectron. 30 (2011) 28–34.
[15] T. Choi, S.H. Kim, C.W. Lee, H. Kim, S.-K. Choi, S.-H. Kim, et al., Synthesis of carbon nanotube–nickel nanocomposites using atomic layer deposition for high-performance non-enzymatic glucose sensing, Biosens. Bioelectron. 63 (2015) 325–330.
[16] X. Xiao, J.R. Michael, T. Beechem, A. McDonald, M. Rodriguez, M.T. Brumbach, et al., Three dimensional nickel–graphene core–shell electrodes, J. Mater. Chem. 22 (2012) 23749–23754.
[17] Z. Wang, Y. Hu, W. Yang, M. Zhou, X. Hu, Facile one-step microwave-assisted route towards Ni nanospheres/reduced graphene oxide hybrids for non-enzymatic glucose sensing, Sensors 12 (2012) 4860–4869.
[18] C.-Y. Ko, J.-H. Huang, S. Raina, W.P. Kang, A high performance non-enzymatic glucose sensor based on nickel hydroxide modified nitrogen-incorporated nanodiamonds, Analyst 138 (2013) 3201–3208.
[19] L.-M. Lu, L. Zhang, F.-L. Qu, H.-X. Lu, X.-B. Zhang, Z.-S. Wu, et al., A nano-Ni based ultrasensitive nonenzymatic electrochemical sensor for glucose: enhancing sensitivity through a nanowire array strategy, Biosens. Bioelectron. 25 (2009) 218–223.
[20] J. Wang, W. Bao, L. Zhang, A nonenzymatic glucose sensing platform based on Ni nanowire modified electrode, Anal. Methods 4 (2012) 4009–4013.
[21] A.K. Geim, K.S. Novoselov, The rise of graphene, Nat. Mater. 6 (2007) 183–191.
[22] S. Stankovich, D.A. Dikin, G.H. Dommett, K.M. Kohlhaas, E.J. Zimney, E.A. Stach, et al., Graphene-based composite materials, Nature 442 (2006) 282–286.
[23] A.C. Neto, F. Guinea, N.M. Peres, K.S. Novoselov, A.K. Geim, The electronic properties of graphene, Rev. Mod. Phys. 81 (2009) 109.
[24] S. Cinti, F. Arduini, Graphene-based screen-printed electrochemical (bio) sensors and their applications: efforts and criticisms, Biosens. Bioelectron. 89 (2017) 107–122.
[25] J.A. Torres, R.B. Kaner, Graphene synthesis: graphene closer to fruition, Nat. Mater. 13 (2014) 328–329.
[26] J. Wang, K.K. Manga, Q. Bao, K.P. Loh, High-yield synthesis of few-layer graphene flakes through electrochemical expansion of graphite in propylene carbonate electrolyte, J. Am. Chem. Soc. 133 (2011) 8888–8891.
[27] X. Liu, P.K. Chu, C. Ding, Surface nano-functionalization of biomaterials, Mater. Sci. Eng. R: Rep. 70 (2010) 275–302.
[28] P.K. Chu, Progress in direct-current plasma immersion ion implantation and recent applications of plasma immersion ion implantation and deposition, Surf. Coat. Technol. 229 (2013) 2–11.
[29] G. Wu, X. Zhang, Y. Zhao, J.M. Ibrahim, G. Yuan, P.K. Chu, Plasma modified Mg–Nd–Zn–Zr alloy with enhanced surface corrosion resistance, Corros. Sci. 78 (2014) 121–129.
[30] C. Liu, Y. Xin, X. Tian, P.K. Chu, Corrosion behavior of AZ91 magnesium alloy treated by plasma immersion ion implantation and deposition in artificial physiological fluids, Thin Solid Films 516 (2007) 422–427.
[31] M. Maitz, R. Poon, X. Liu, M.-T. Pham, P.K. Chu, Bioactivity of titanium following sodium plasma immersion ion implantation and deposition, Biomaterials 26 (2005) 5465–5473.
[32] R. Reis, L.F. Dumée, B.L. Tardy, R. Dagastine, J.D. Orbell, J.A. Schutz, et al., Towards enhanced performance thin-film composite membranes via surface plasma modification, Sci. Rep. 6 (2016) 29206.
[33] T. Makabe, Z.L. Petrovic, Plasma Electronics: Applications in Microelectronic Device Fabrication, CRC Press, 2014.
[34] T. Gokus, R. Nair, A. Bonetti, M. Bohmler, A. Lombardo, K. Novoselov, et al., Making graphene luminescent by oxygen plasma treatment, ACS Nano 3 (2009) 3963–3968.
[35] N. Xiao, X. Dong, L. Song, D. Liu, Y. Tay, S. Wu, et al., Enhanced thermopower of graphene films with oxygen plasma treatment, ACS Nano 5 (2011) 2749–2755.
[36] R.I. Jafri, N. Rajalakshmi, S. Ramaprabhu, Nitrogen doped graphene nanoplatelets as catalyst support for oxygen reduction reaction in proton exchange membrane fuel cell, J. Mater. Chem. 20 (2010) 7114–7117.
[37] N. Peltekis, S. Kumar, N. McEvoy, K. Lee, A. Weidlich, G.S. Duesberg, The effect of downstream plasma treatments on graphene surfaces, Carbon 50 (2012) 395–403.
[38] M. Chen, H. Zhou, C. Qiu, H. Yang, F. Yu, L. Sun, Layer-dependent fluorination and doping of graphene via plasma treatment, Nanotechnology 23 (2012) 115706.
[39] M. Rybin, A. Pereyaslavtsev, T. Vasilieva, V. Myasnikov, I. Sokolov, A. Pavlova, et al., Efficient nitrogen doping of graphene by plasma treatment, Carbon 96 (2016) 196–202.
[40] S.-J. Li, N. Xia, X.-L. Lv, M.-M. Zhao, B.-Q. Yuan, H. Pang, A facile one-step electrochemical synthesis of graphene/NiO nanocomposites as efficient electrocatalyst for glucose and methanol, Sens. Actuators B: Chem. 190 (2014) 809–817.
[41] N. Hui, S. Wang, H. Xie, S. Xu, S. Niu, X. Luo, Nickel nanoparticles modified conducting polymer composite of reduced graphene oxide doped poly(3,4-ethylenedioxythiophene) for enhanced nonenzymatic glucose sensing, Sens. Actuators B: Chem. 221 (2015) 606–613.
[42] B. Yuan, C. Xu, D. Deng, Y. Xing, L. Liu, H. Pang, et al., Graphene oxide/nickel oxide modified glassy carbon electrode for supercapacitor and nonenzymatic glucose sensor, Electrochim. Acta 88 (2013) 708–712.
[43] M. Fleischmann, K. Korinek, D. Pletcher, The oxidation of organic compounds at a nickel anode in alkaline solution, J. Electroanal. Chem. Interfacial Electrochem. 31 (1971) 39–49.
[44] I. Danaee, M. Jafarian, F. Forouzandeh, F. Gobal, M.G. Mahjani, Impedance spectroscopy analysis of glucose electro-oxidation on Ni-modified glassy carbon electrode, Electrochim. Acta 53 (2008) 6602–6609.
[45] Y.F. Yuan, X.H. Xia, J.B. Wu, J.L. Yang, Y.B. Chen, S.Y. Guo, Nickel foam-supported porous Ni(OH)2/NiOOH composite film as advanced pseudocapacitor material, Electrochim. Acta 56 (2011) 2627–2632.
[46] Y. Miao, L. Ouyang, S. Zhou, L. Xu, Z. Yang, M. Xiao, et al., Electrocatalysis and electroanalysis of nickel, its oxides, hydroxides and oxyhydroxides toward small molecules, Biosens. Bioelectron. 53 (2014) 428–439.
[47] J. Yang, J.-H. Yu, J.R. Strickler, W.-J. Chang, S. Gunasekaran, Nickel nanoparticle–chitosan-reduced graphene oxide-modified screen-printed electrodes for enzyme-free glucose sensing in portable microfluidic devices, Biosens. Bioelectron. 47 (2013) 530–538.
[48] A.J. Bard, L.R. Faulkner, J. Leddy, C.G. Zoski, Electrochemical Methods: Fundamentals and Applications, Wiley, New York, 1980.
[49] P. Suneesh, K. Chandhini, T. Ramachandran, B.G. Nair, T.S. Babu, Tantalum oxide honeycomb architectures for the development of a non-enzymatic glucose sensor with wide detection range, Biosens. Bioelectron. 50 (2013) 472–477.
[50] L. Nagy, G. Nagy, Spectroscopic confirmation of electrocatalytic behavior of amperometric carbohydrate detection on copper electrode, Microchem. J. 84 (2006) 70–74.
[51] H. Tian, M. Jia, M. Zhang, J. Hu, Nonenzymatic glucose sensor based on nickel ion implanted-modified indium tin oxide electrode, Electrochim. Acta 96 (2013) 285–290.
[52] C. Zhao, C. Shao, M. Li, K. Jiao, Flow-injection analysis of glucose without enzyme based on electrocatalytic oxidation of glucose at a nickel electrode, Talanta 71 (2007) 1769–1773.
[53] S. Ci, T. Huang, Z. Wen, S. Cui, S. Mao, D.A. Steeber, et al., Nickel oxide hollow microsphere for non-enzyme glucose detection, Biosens. Bioelectron. 54 (2014) 251–257.
[54] A. Sun, J. Zheng, Q. Sheng, A highly sensitive non-enzymatic glucose sensor based on nickel and multi-walled carbon nanotubes nanohybrid films fabricated by one-step co-electrodeposition in ionic liquids, Electrochim. Acta 65 (2012) 64–69.
[55] L. Zheng, J.-q. Zhang, J.-f. Song, Ni (II)–quercetin complex modified multiwall carbon nanotube ionic liquid paste electrode and its electrocatalytic activity toward the oxidation of glucose, Electrochim. Acta 54 (2009) 4559–4565.
[56] Z. Liu, Y. Guo, C. Dong, A high performance nonenzymatic electrochemical glucose sensor based on polyvinylpyrrolidone–graphene nanosheets–nickel nanoparticles–chitosan nanocomposite, Talanta 137 (2015) 87–93.
[57] Y. Ding, Y. Wang, L. Su, M. Bellagamba, H. Zhang, Y. Lei, Electrospun Co3O4 nanofibers for sensitive and selective glucose detection, Biosens. Bioelectron. 26 (2010) 542–548.
[58] X.-Y. Lang, H.-Y. Fu, C. Hou, G.-F. Han, P. Yang, Y.-B. Liu, et al., Nanoporous gold supported cobalt oxide microelectrodes as high-performance electrochemical biosensors, Nat. Commun. 4 (2013) 2169.
[59] L. Zhang, D. Manuzzi, H.V.E. de los Monteros, W. Jia, D. Huo, et al., Ultrasensitive and selective non-enzymatic glucose detection using copper nanowires, Biosens. Bioelectron. 31 (2012) 426–432.
[60] H.S. Fogler, Elements of Chemical Reaction Engineering, 1999.
[61] Y. Zhang, Y. Wang, J. Jia, J. Wang, Nonenzymatic glucose sensor based on graphene oxide and electrospun NiO nanofibers, Sens. Actuators B: Chem. 171 (2012) 580–587.
[62] Z. Shen, W. Gao, P. Li, X. Wang, Q. Zheng, H. Wu, et al., Highly sensitive nonenzymatic glucose sensor based on Nickel nanoparticle–attapulgite-reduced graphene oxide-modified glassy carbon electrode, Talanta 159 (2016) 194–199.
[63] B. Wang, S. Li, J. Liu, M. Yu, Preparation of nickel nanoparticle/graphene composites for non-enzymatic electrochemical glucose biosensor applications, Mater. Res. Bull. 49 (2014) 521–524.
[64] S. Park, H. Boo, T.D. Chung, Electrochemical non-enzymatic glucose sensors, Anal. Chim. Acta 556 (2006) 46–57.
[65] S. Hrapovic, J.H.T. Luong, Picoamperometric detection of glucose at ultrasmall platinum-based biosensors: preparation and characterization, Anal. Chem. 75 (2003) 3308–3315.

Biographies

Hao Wu is currently studying as a Ph.D. student in Department of Physics and Materials Science, City University of Hong Kong under the supervision of Professor Paul. K. Chu. His research interests are focused on electrochemical biosensors, corrosion science, and biomaterials.

Yu Yu obtained his PhD degree in materials science from the Institute of Chemistry, Chinese Academy of Sciences (ICCAS) in 2014. He is currently a researcher of Prof. Kejian Ding's group at Beijing Jiaotong University (BJTU), with the research interests including the development of nanostructured materials for energy storage, and photocatalysis/electrocatalysis in preparation of clean energy.

Wenyu Gao received her BS degree in bioinformatics science from Zhengzhou University in 2014. Now she is a Master Candidate in the school of science at Beijing Jiaotong University. Her research interests focus on the preparation of novel nanomaterials for energy catalysis and electrical chemistry.

Ang Gao is pursuing his Ph.D. in Department of Physics and Materials Science, City University of Hong Kong under the supervision of Professor Paul K. Chu. His research interests include surface modification of titanium and its alloys for biomedical applications.

Abdul Mateen Qasim is pursuing his Ph.D. in Department of Physics and Materials Science, City University of Hong Kong under the supervision of Professor Paul K. Chu. His research interests include plasma technology and functional coatings.

Fan Zhang received his master degree in Southwest Institute of Physics and currently works as a research assistant in plasma lab, City University of Hong Kong. His research interests include applications of low temperature plasma.

Junzhong Wang received his Ph.D. in Chemistry at University of Science & Technology of China. He has worked as Postdoc in National Institute of Advanced Industrial Science & Technology (AIST), Japan and as Research Fellow in National University of Singapore. Currently, he is Professor in Institute of Coal Chemistry, Chinese Academy of Sciences. His research interests include: (1) Application of graphene materials synthesized via green electrochemical approaches; (2) Rational synthesis for advanced films, membranes and nanocomposites of graphene; (3) Electrochemical energy storage: supercapacitors, batteries and electrocatalysts for O_2 reduction.

Kejian Ding obtained his PhD degree in Biophysics from the Institute of Plasma Physics, Chinese Academy of Sciences (IPPCAS) in 2006. Currently, he is Chair of Department of Physics, Beijing Jiaotong University. His research focuses on the design, synthesis and properties of various inorganic-organic nanostructures and their application in energy and biosensor applications.

Guosong Wu received his PhD in materials processing engineering from Shanghai Jiao Tong University (China) in 2007. He has worked as a researcher in Chinese Academy of Sciences, City University of Hong Kong and Kwangwoon University (South Korea) for about 10 years. Presently, he is Professor in College of Mechanics and Materials at Hohai University (China). His research interests include surface engineering, thin solid films, and plasma related technologies.

Paul K. Chu received his Ph.D. in chemistry from Cornell University and is presently Chair Professor of Materials Engineering in City University of Hong Kong. His research activities encompass plasma surface engineering and materials science. He is Chairman of the Plasma-Based Ion Implantation (PBII&D) International Committee, a member of the Ion Implantation Technology (IIT) International Committee and IEEE Nuclear and Plasma Science Society Fellow Evaluation Committee, senior editor of IEEE Transactions on Plasma Science, and associate editor of Materials Science and Engineering Reports. He is Fellow of the APS, AVS, IEEE, MRS, and HKIE.

Supporting Information

Nickel plasma modification of graphene for high-performance non-enzymatic glucose sensing

Hao Wu [1], Yu Yu [2], Wenyu Gao [2], Ang Gao [1], Abdul Mateen Qasim [1], Junzhong Wang [3], Kejian Ding [2*], Guosong Wu [1], Paul K. Chu [1†]

[1] *Department of Physics and Materials Science, City University of Hong Kong, Tat Chee Avenue, Kowloon, Hong Kong, China*

[2] *College of Life sciences and Bioengineering, Beijing Jiaotong University, Beijing 100044, PR China*

[3] *Key Laboratory of Carbon Materials, Institute of Coal Chemistry, Chinese Academy of Science, Taiyuan, 030001, P R China*

[*]Corresponding author :

E-mail: dkjian@bjtu.edu.cn (Kejian Ding)

[†]Corresponding author :

E-mail: paul.chu@cityu.edu.hk (P. K. Chu)

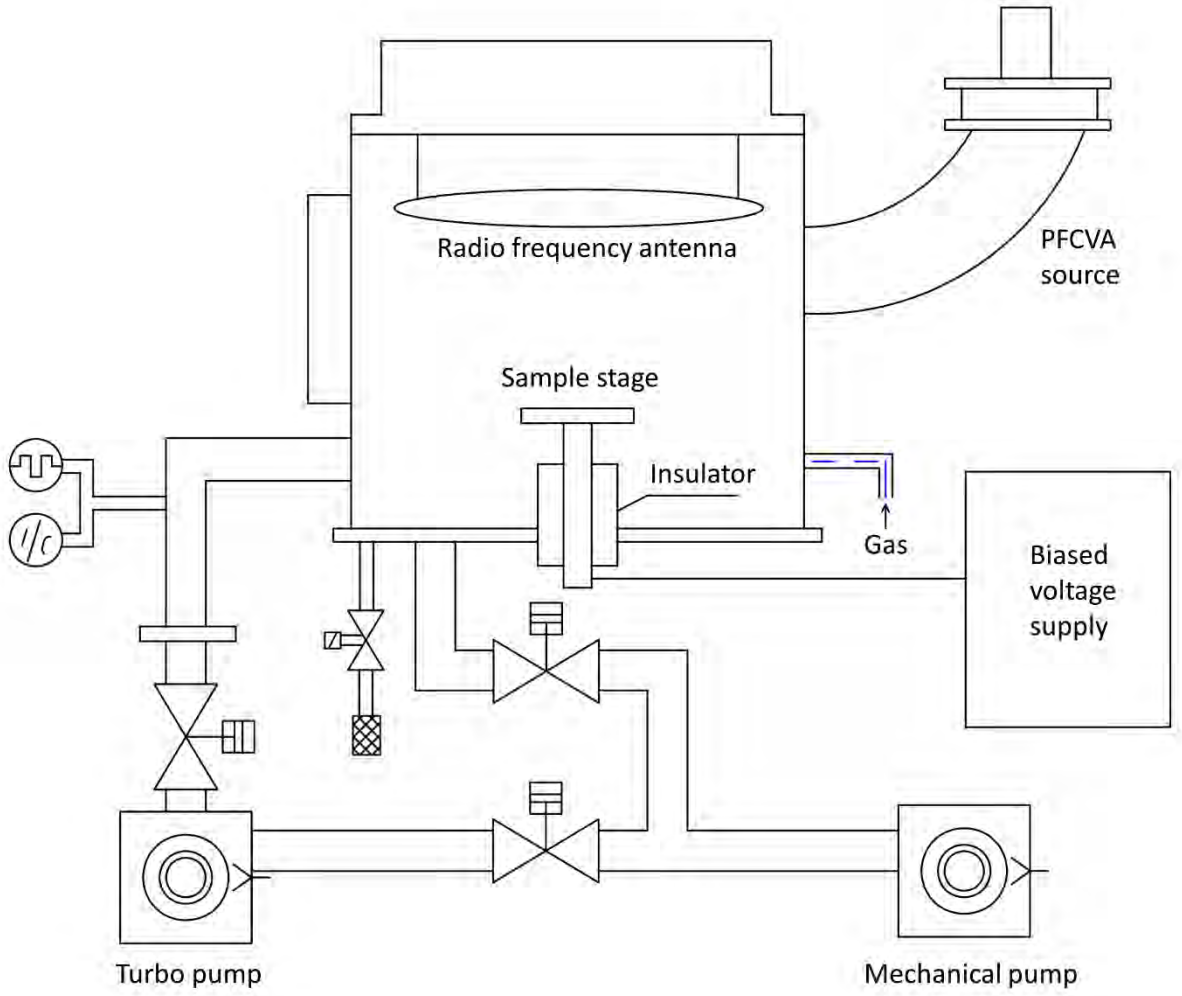

Figure S1. Schematic illustration of the PIII&D system.

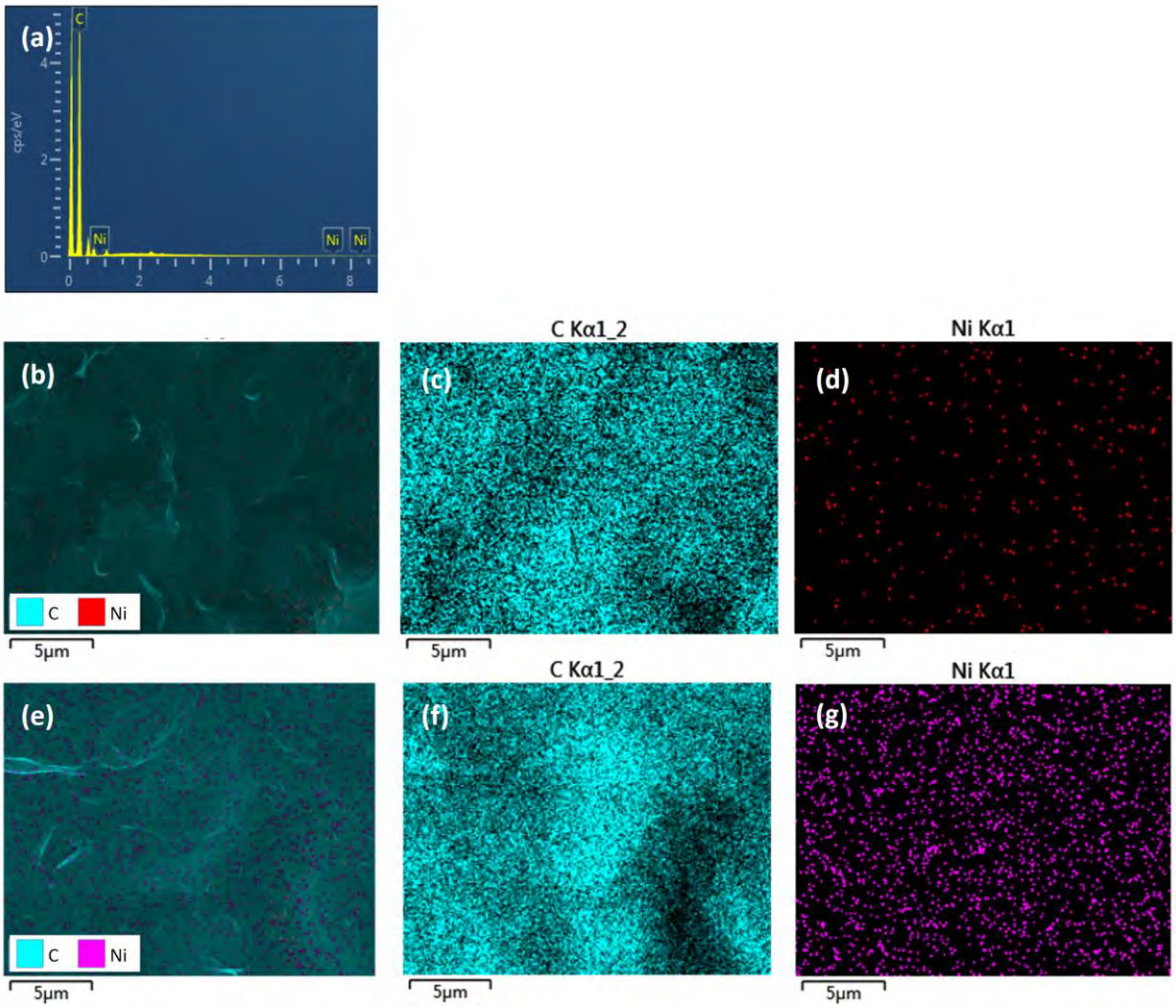

Figure S2. (a) EDS scan of the untreated graphene; (b)-(d) EDS maps of the untreated graphene; (e)-(g) EDS maps of the Ni plasma-treated graphene.

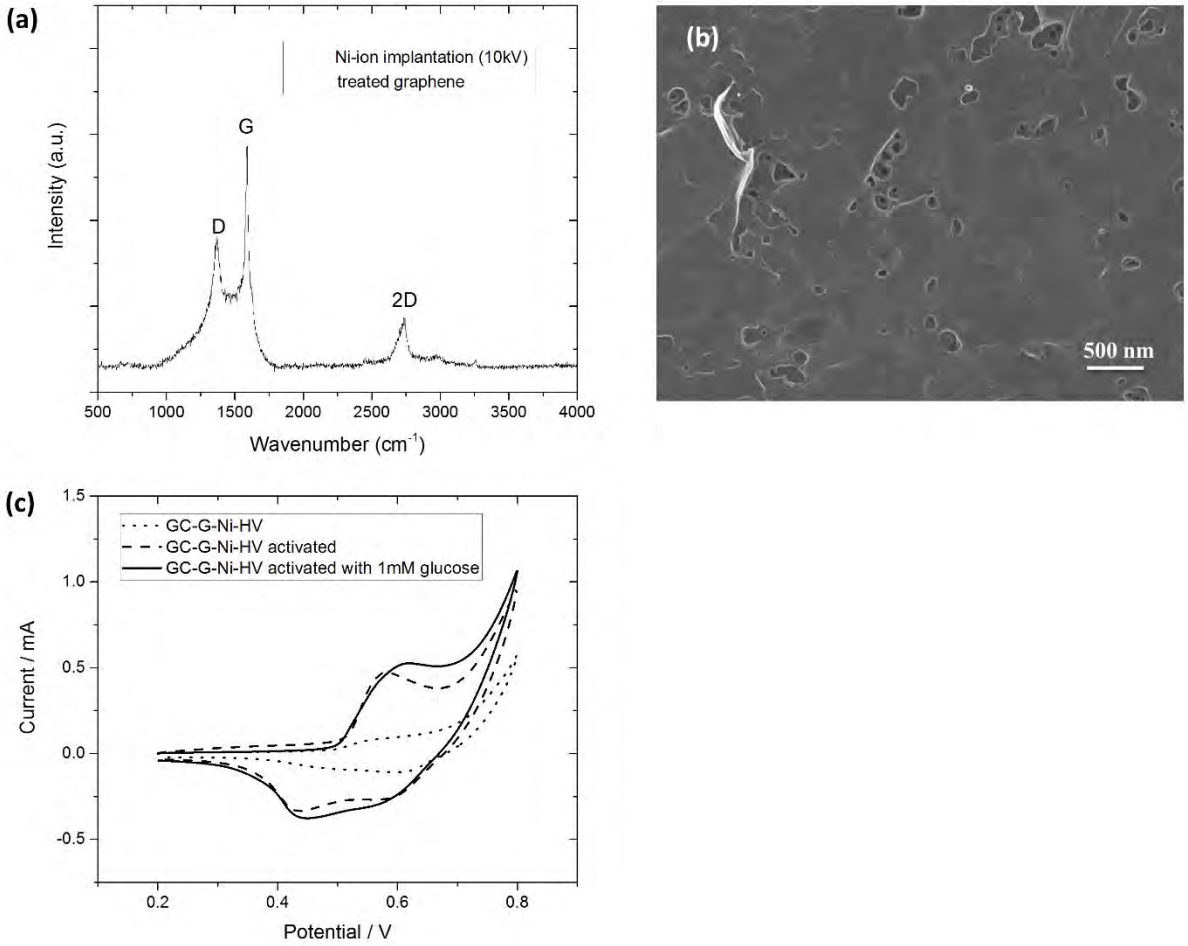

Figure S3. (a) Raman scattering spectrum of graphene after high-energy Ni ion implantation (10 kV); (b) Surface morphology of the sample shown in (a); (c) Cyclic voltammograms of the GC-G-Ni-HI electrode at a scanning rate of 100 mV/s.

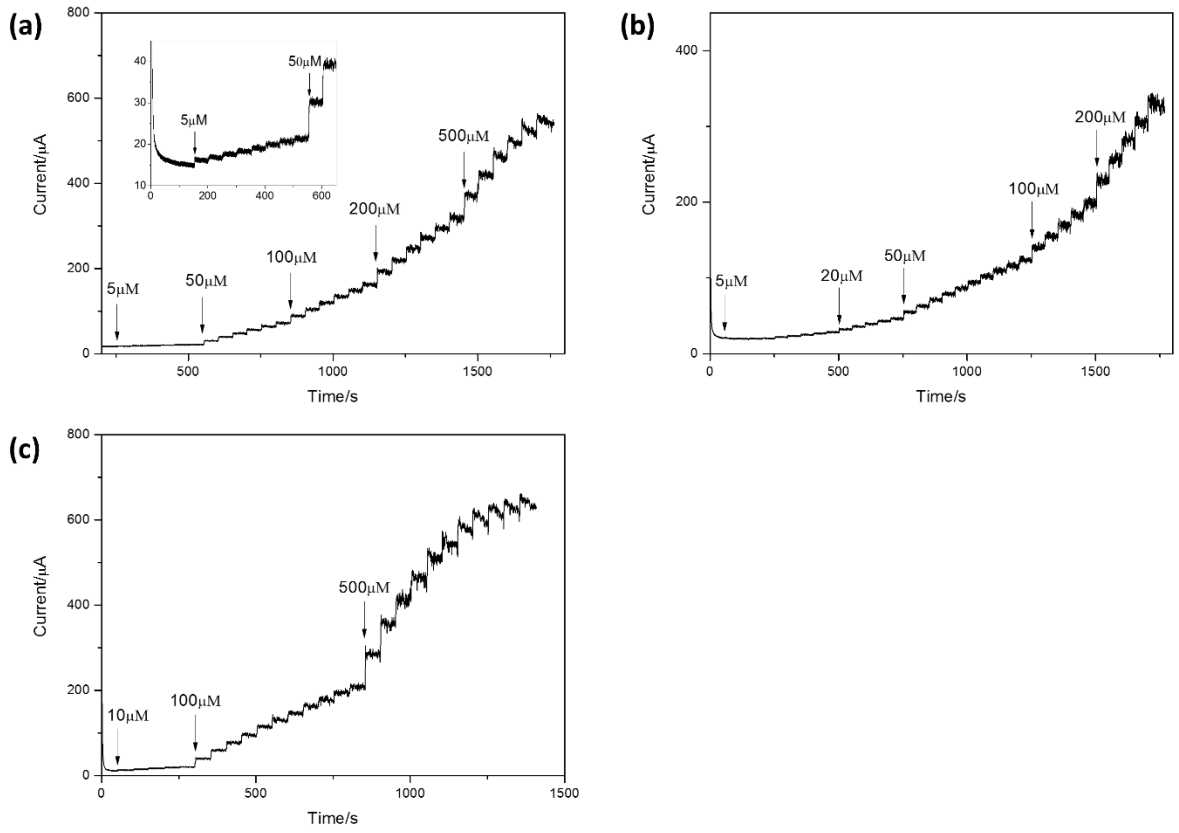

Figure S4. Amperometric current response plots of 3 different GCE-G-Ni electrodes in 1 batch after addition of glucose at an applied potential of 0.6 V. The current response is calculated from 4 independently prepared electrodes.

Table S1. Fitted EIS results of GC, GC-G, GC-Ni, GC-G-Ni based on the corresponding equivalent circuit models.

	GC	**GC-G**	**GC-Ni**	**GC-G-Ni**
R_s (ohm*cm^{-2})	60.33±0.43	68.1±0.35	65.02±0.18	68.5±0.22
Y_1 (ohm^{-2}*cm^{-2}*S^{-n})	(1.06±0.053)*10^{-6}	(1.17±0.12)*10^{-4}	(1.73±0.05)*10^{-4}	(7.85±0.053)*10^{-5}
n_1	0.9274±0.0053	0.6585±0.0123	0.6221±0.0041	0.7204±0.0086
R_{ct} (ohm*cm^{-2})	554.3±9.4	141.8±6.8	339.5±7.7	95.6±2.0
Y_2(ohm^{-2}*cm^{-2}*S^{-n})	(3.78±0.138)*10^{-3}	(3.25±0.047)*10^{-3}	(4.28±0.098)*10^{-3}	(5.56±0.050)*10^{-3}
n_2	0.3069±0.0214	0.4115±0.0107	0.4393±0.0145	0.4428±0.0070
χ^2	4.991*10^{-4}	2.582*10^{-4}	8.696*10^{-5}	1.131*10^{-4}